Chapter 12

Convective Mass Transfer in a Champagne Glass

Fabien Beaumont, Gérard Liger-Belair and Guillaume Polidori

Additional information is available at the end of the chapter

http://dx.doi.org/10.5772/51956

1. Introduction

Legend has it that the Benedictine monk Dom Pierre Pérignon discovered the Champagne method for making sparkling wines more than 300 years ago. As it happens, a paper presented to the Royal Society in London described the Champagne production method in 1662, six years before Pérignon ever set foot in a monastery. In fact, Pérignon was first tasked with keeping bubbles out of wine, as the effervescence was seen as vulgar at the time. But then tastes changed and fizz became fashionable, so Pérignon's mandate was reversed; he went on to develop many advances in Champagne production, including ways to increase carbonation. In any case, the process was not regularly used in the Champagne region of France to produce sparkling wine until the 19th century. Since that time, Champagne has remained the wine of celebration, undoubtedly because of its bubbling behavior.

But what is the exact role of the bubbles? Is it just aesthetics? Do they contribute to only one aspect, or to many aspects, of the subjective final taste? We have been rigorously analyzing Champagne for more than a decade, using the physics of fluids in the service of wine in general and Champagne- tasting science in particular.

2. The Champagne method

Fine sparkling wines and Champagne result from a two-step fermentation process. After completion of the first alcoholic fermentation, some flat Champagne wine (called base wine) is bottled with a mixture of yeast and sugar. Consequently, a second fermentation starts inside the bottle as the yeast consumes the sugar, producing alcohol and a large amount of carbon dioxide (CO_2). This is why Champagne has a high concentration of CO_2 dissolved in

it about 10 grams per liter of fluid and the finished Champagne wine can be under as much as five or six atmospheres of pressure. As the bottle is opened, the gas gushes out in the form of tiny CO_2 bubbles. In order for the liquid to regain equilibrium once the cork is removed, it must release about five liters of CO_2 from a 0.75 liter bottle, or about six times its own volume. About 80 percent of this CO_2 is simply outgassed by direct diffusion, but the remaining 20 percent still equates to about 20 million bubbles per glass (a typical flute holds about 0.1 liter). For Champagne connoisseurs, smaller bubble size is also a measure of quality.For consumers and winemakers as well, the role usually ascribed to bubbles in Champagne tasting is to awaken the sight sense. Indeed, the image of Champagne is intrinsically linked to the bubbles that look like "chains of pearls" in the glass and create a cushion of foam on the surface. But beyond this visual aspect, the informed consumer recognizes effervescence as one of the main ways that flavor is imparted, because bursting CO_2 bubbles propel the aroma of sparkling wine into the drinker's nose and mouth (Figure 1).

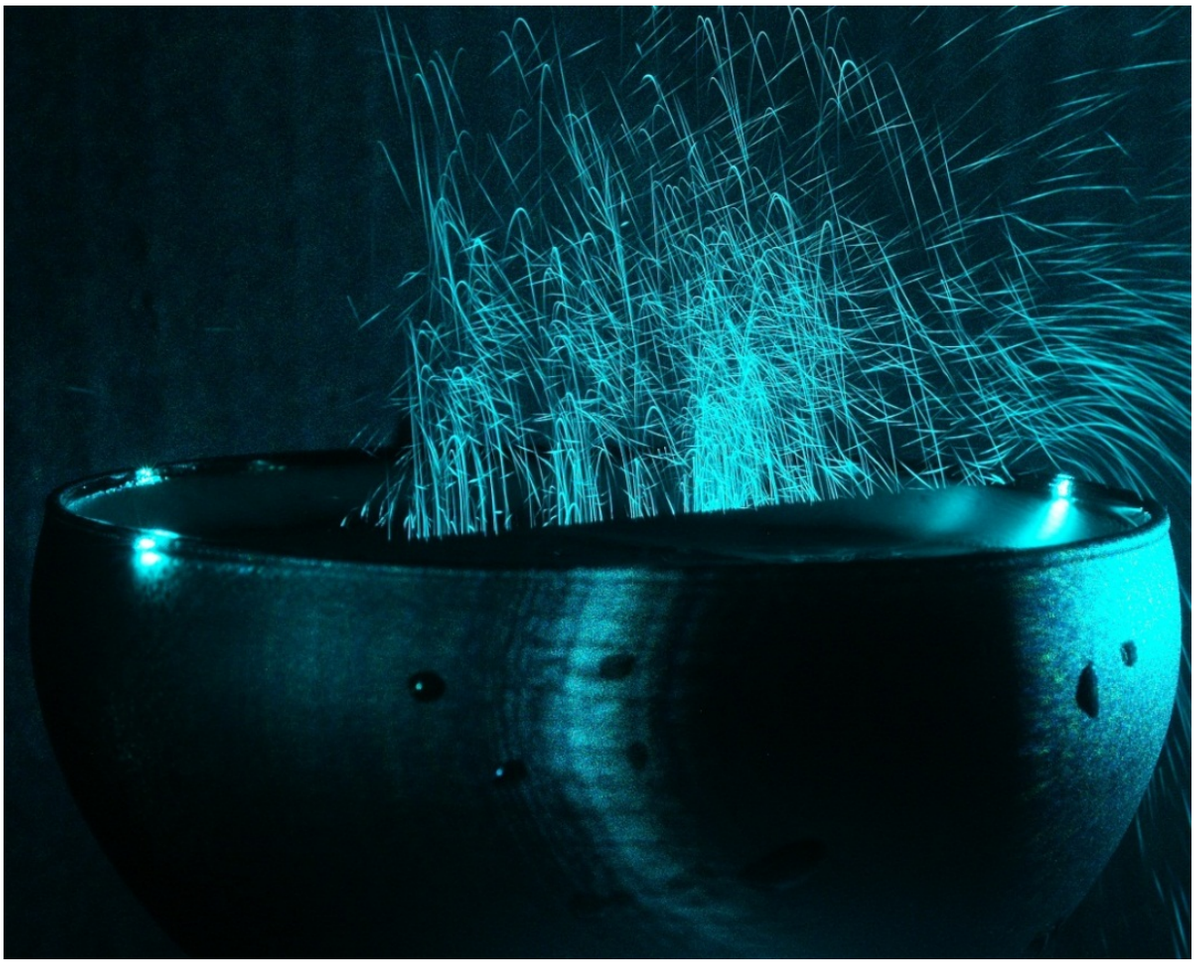

Figure 1. A glass of Champagne is a feast for all the senses; indeed it is sight and sound that make sparkling wines particularly special. Elegant bubble trains rise from nucleation sites suspended in the fluid *(right).* Bubbles reaching the top of the glass burst and produce a fog of droplets *(above).* The questions being explored by enologists include how the carbonation and effervescence induce fluid flow in, and affect the flavor of, the beverage. (All photographs are courtesy of the authors.)

http://dx.doi.org/10.5772/51956

One cannot understand the bubbling and aromatic exhalation events in champagne tasting, however, without studying the flow-mixing mechanisms inside the glass. Indeed, a key assumption is that a link of causality may exist between flow structures created in the wine due to bubble motion and the process of flavor exhalation [1]. But the consequences of the bubble behavior on the dynamics of the Champagne inside the glass and the CO_2 propelling process are still unknown. Quantifying the exhalation of flavors and aromas seems a considerable challenge, something that is difficult to control experimentally, but this constitutes the aim of our current work.

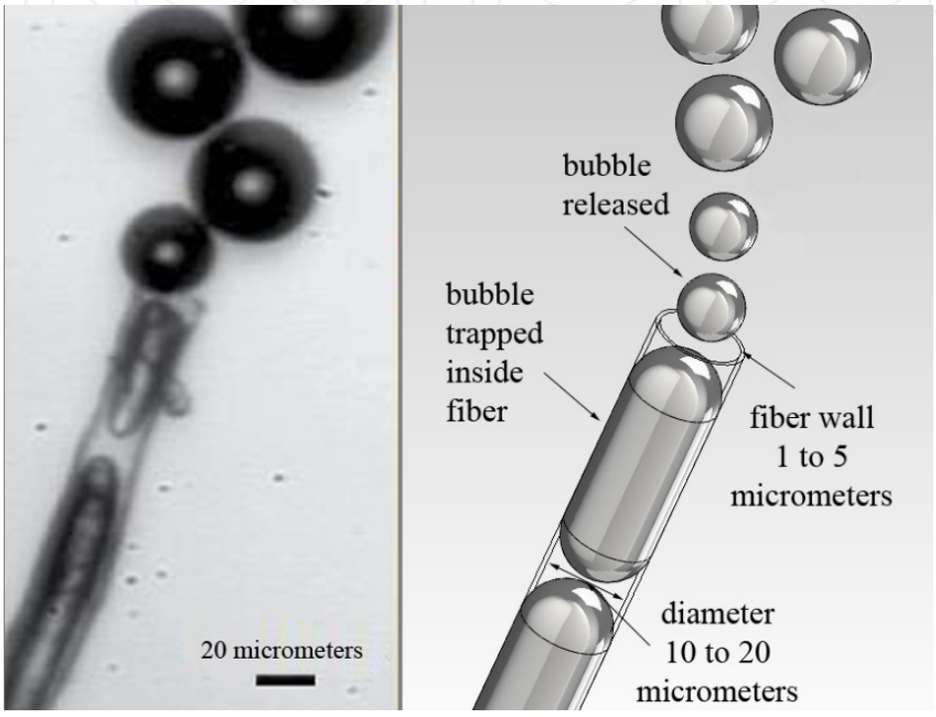

Figure 2. Bubbles in sparkling wines do not spring into existence unaided, but require a starting point. These nucleation sites take the form of microscopic cellulose fibers, from the air or a towel used to dry the glass, which trap air pockets as the glass is filled. Carbon dioxide from the wine diffuses into the gas pockets, producing bubbles like clockwork *(left)*.

3. The birth of bubbles

The first step is to elucidate how bubbles themselves come into being. Generally speaking, two ways exist, and sometimes coexist, to generate bubble chains in Champagne glasses [2-6]. Natural effervescence depends on a random condition: the presence of tiny cellulose fibers deposited from the air or left over after wiping the glass with a towel, which cling to the glass due to electrostatic forces (Figure 2). These fibers are made of closely packed microfibrils, themselves consisting of long polymer chains composed mainly of glucose. Each fiber, about 100 micrometers long, develops an internal gas pocket as the glass is filled. Capillary action tries to pull the fluid inside the micro-channel of the fiber, but if the fiber is

completely submerged before it can be filled, it will hold onto its trapped air. Such gas trapping is aided when the fibers are long and thin, and when the liquid has a low surface tension and high viscosity. Champagne has a surface tension about 30 percent less than that of water, and a viscosity about 50 percent higher.

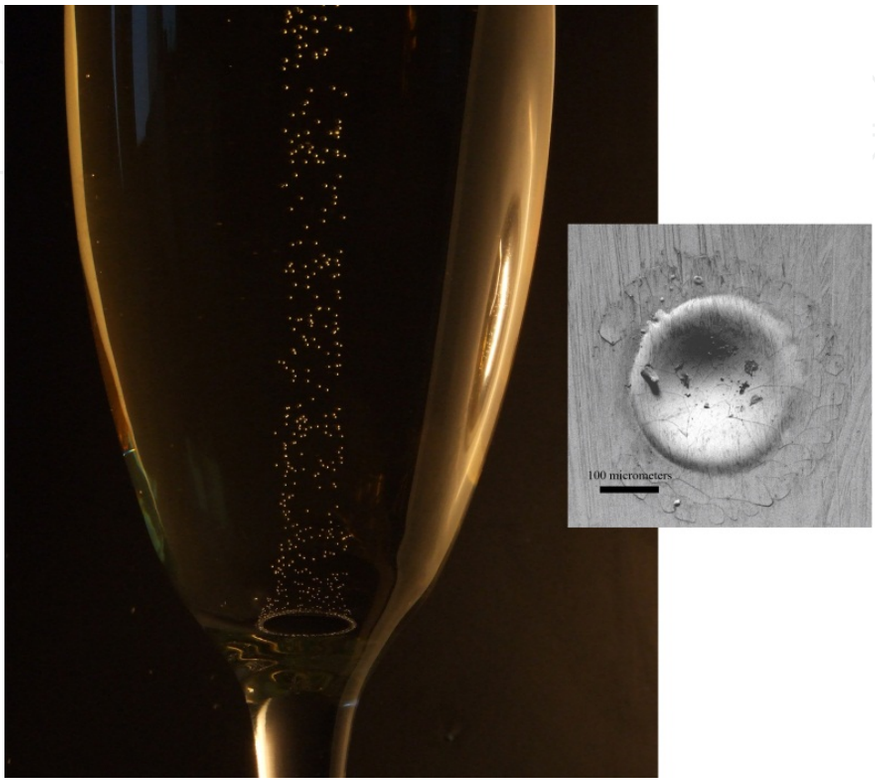

Figure 3. In order to study effervescence in Champagne and other sparkling wines, random bubble production must be replaced with controlled creation of bubble streams. The glass bottom is etched with a ring that provides nucleation sites for regular bubble trains *(left).* The ring consists of many small impact points *(right)* from a laser, one of which is shown above. Glasses etched with a single nucleation point were used in studies to see how a single stream of bubbles would induce motion in the surrounding fluid, and what shape that fluid motion would take.

These microfiber gas pockets act as nucleation sites for the formation of bubbles. To aggregate, CO_2 has to push through liquid molecules held together by van der Waals forces, which it would not have enough energy to do on its own. The gas pockets lower the energy barrier to bubble formation (as long as they are above a critical size of 2 micrometers in radius, because below that size the gas pressure inside the bubble is too high to permit CO_2 to diffuse inside). It should be noted that irregularities in the glass surface itself cannot act as nucleation sites such imperfections are far too small, unless larger micro scratches are purposely made. Once a bubble grows to a size of 10 to 50 micrometers, it is buoyant enough to detach from the fiber, and another one forms like clockwork; an average of 30 bubbles per second are released from each fiber. The bubbles expand from further diffusion of CO_2 into them as they rise, which increases their buoyancy and accelerates their speed of ascent [2, 5-6]. They usually max out at less than a millimeter in diameter over the course of their one- to five-second travel time up the length of a flute. Because natural nucleation is very random

http://dx.doi.org/10.5772/51956

and not easily controllable, another way to generate bubbles is to use a mechanical process that is perfectly reproducible from one filling to the next. Glassmakers use a laser to engrave artificial nucleation sites at the bottom of the glass; such modified glasses are commonly used by Champagne houses during tastings (Figure 3). To make the effervescence pattern pleasing to the eye, artisans use no fewer than 20 impacts to create a ring shape, which produces a regular column of rising bubbles [3-5, 7].

4. Fizz and flow

The displacement of an object in a quiescent fluid induces the motion of fluid layers in its vicinity. Champagne bubbles are no exception to this rule, acting like objects in motion, no matter whether the method used to produce them was random or artificial. Viscous effects make the lower part of a bubble a low-pressure area, which attracts fluid molecules around it and drags some fluid to the top surface, although the bubbles move about 10 times faster than the fluid (Figure 4). Consequently, bubbles and their neighboring liquid move as concurrent upward flows along the center line of the glass. Because the bubble generation from nucleation sites is continuous, and because a glass of Champagne is a confined vessel, this constant upward ascent of the fluid ineluctably induces a rotational flow as well [2-5, 7-8]. To get a precise idea of the role bubbles play in the fluid motion, we observed a Champagne flute with single nucleation site at the bottom (Figure 4). A bubble's geometric evolution is well studied in carbonated beverages. For example, we know that the bubble growth rate during vertical ascent reliably leads to an average diameter of about 500 micrometers for a 10 centimeter migration length in a flute. In fact, for such a liquid supersaturated with dissolved CO_2 gas molecules, empirical relationships reveal the bubble diameter to be proportional to the cube root of the vertical displacement. Another property of bubbles is that they can act as either rigid or flexible spheres as they rise, depending on the content of the fluid they are in, and rigid spheres experience more drag than flexible ones. Champagne bubbles do not act as rigid spheres, whereas bubbles in other fizzy fluids, such as beer, do. Beer contains a lot of proteins, which coat the outside of the bubbles as they ascend, preventing their deformation. Beer is also less carbonated than Champagne, so bubbles in it do not grow as quickly, making it easier for proteins to completely encircle them. But Champagne is a relatively low-protein fluid, so there are fewer surfactants to stick to the bubbles and slow them down as they ascend. In addition, Champagne's high carbonation makes bubbles grow rapidly on their upwards trip, creating ever more untainted surface area, in effect cleaning themselves of surfactants faster than new molecules can fill in the space. However, some surfactants are necessary to keep bubbles in linear streams with none; fluid flows would jostle the bubbles out of their orderly lines.

We carried out filling experiments at room temperature to avoid condensation on the glass surface, and allowed the filled glass to settle for a minute or so before taking measurements [2-5, 7-9]. Our visualization is based on a laser tomography technique, where a laser sheet 2 millimeters wide crosses the center line of the flute, imaging just this two- dimensional section of the glass using long-exposure photography. To avoid optical distortions by the

curved surface of the glass, this latter is partially immersed in a parallelepiped tank full of water (Figure 5) with a refractive index close to that of champagne (RI champagne 1.342 while RI pure water 1.332).

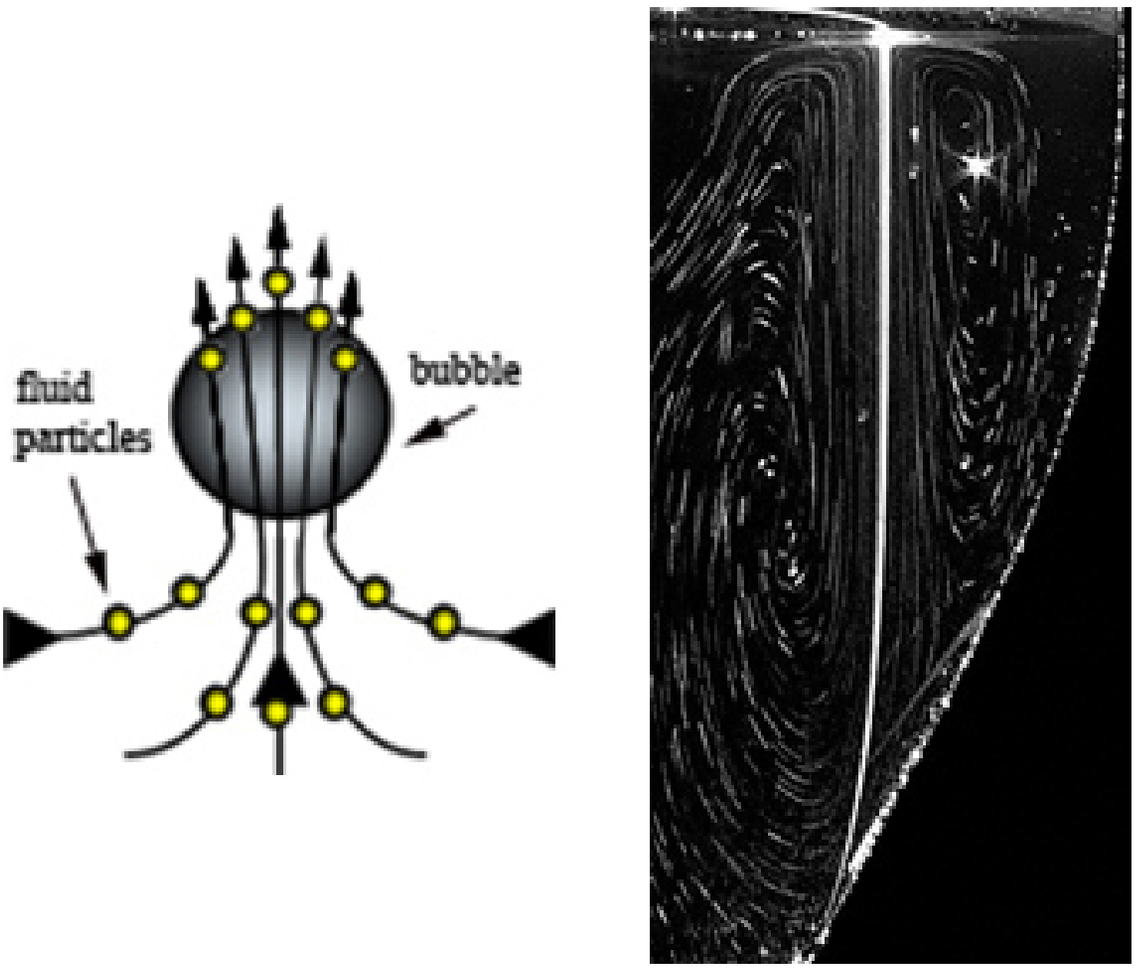

Figure 4. The fluid motion occurs because as the bubbles rise, they drag the fluid along in their wake (left). When seeded with tiny polymer particles and imaged in a time-lapse photo with a laser, the bubble stream appears as a white line, and the regular ring vortex of movement induced in the fluid from the bubble movement is clearly outlined by the particles (right).

We seeded the Champagne with Rilsan particles as tracers of fluid motion. These polymer particles are quasi-spherical in shape, with diameters ranging from 75 to 150 micrometers, and have a density (1.060) close to that of Champagne (0.998). The particles are neutrally buoyant and do not affect bubble production, but they are very reflective of laser light. It is amazing to see the amount of fluid that can be set in motion by viscous effects. In our resulting images, a central line corresponds to the bubble train path during the exposure time of the camera, and the fluid motion is characterized by a swirling vortex that is symmetrical on both sides of the bubble chain (Figure 6). The vortex-pair in the planar view of our image can be extrapolated to show a three-dimensional annular flow around the center line of bub-

http://dx.doi.org/10.5772/51956

bles (Figure 6). This means that a single fixed nuclear site on the glass surface can set the entire surrounding fluid into a small-scale ring vortex.

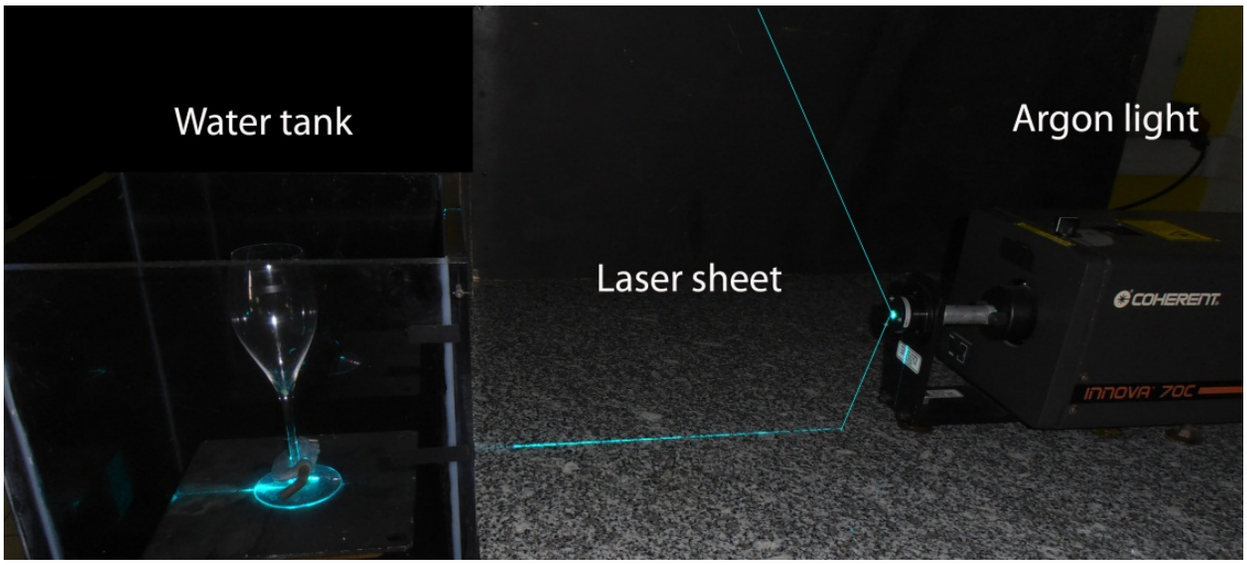

Figure 5. Experimental set-up

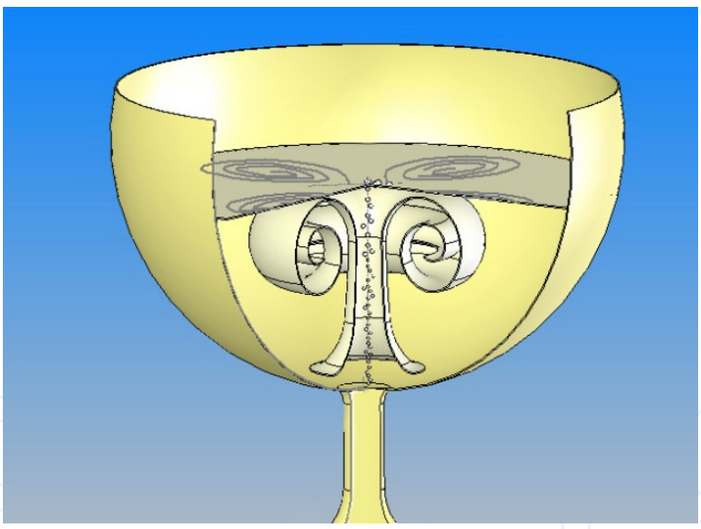

Figure 6. Illustration of the three-dimensional flow in an engraved coupe-glass (right).

5. Controlled mixing

Champagne-tasting science involves a number of very subjective judgments, often difficult to quantify. For example, there is an inherent compromise between the visual aspects of bubbly behavior and olfactory stimulation, as these two qualities appear to be at odds. Too

much nucleation will excite the sense of sight but cause the carbonation to quickly fizzle out, making for unpleasant tasting. On the contrary, poor nucleation will produce fewer bubbles in the glass, but more bubbles and aromas in the taster's nose and mouth, consequently enhancing the senses of smell and taste at the expense of sight. From the many experiments we have conducted with controlled effervescence, it seems that an ideal number of about 20 nucleation sites best satisfies this dilemma. Our laser visualizations of fluid flow have shown that a flute with an engraved circular crown reaches a steady state of fluid motion about 30 seconds after the glass is poured [2-5, 7-8]. The vortices do not swirl around and change shape, in contrast to those created in unetched glasses. The bubbles are highly reflective, allowing one to clearly observe the formation of a rising gas column along the vertical glass axis from the treated bottom up to the free surface of the beverage. Consequently, the driving force it imparts to the surrounding fluid generates two large counter-rotating vortices in the vertical lighted section (Figure 6-7). These cells are located outside the rising bubbles, close to the wall of the flute. Because this gas column acts like a continuous swirling-motion generator within the glass, the flow structure exhibits a quasi-steady two-dimensional behavior with a geometry that is symmetrical around the center line of the glass. It clearly appears in the case of an engraved flute that the whole domain of the liquid is homogeneously mixed (Figure 7, right). To complete our observations, we also studied the flow in an engraved traditional Champagne coupe, which is much wider but shallower than the flute. As in the flute, the rising CO_2 bubble column causes the main fluid to move inside the coupe. However, two distinctive steady-flow patterns, instead of one, appear in a glass of this shape. Like the flute, the coupe clearly exhibits a single swirling ring, whose cross section appears as two counter- rotating vortices close to the glass axis. What strongly differs from the motion in the flute is that this recirculation flow region does not occupy the whole volume of the glass. The periphery of the coupe is instead characterized by a zone of no motion. Thus, for a wide-rimmed glass, only about half of the liquid bulk participates in the Champagne mixing process. Nevertheless, in an engraved glass of either shape, the presence of a ring vortex is not time-dependent; it still forms in the coupe, despite the ascent time being about a third of that in the flute.

6. Infrared imaging technique used to visualize the flow of gaseous CO_2 desorbing from champagne

A visualization technique based on the Infrared (IR) thermography principle has been used to film the gaseous CO_2 fluxes outgassing from champagne (invisible in the visible light spectrum) [10]. The CO_2 absorptions observable by the IR camera are quite weak because this gas molecule has only a strong absorption peak in the detector bandwidth at 4.245 mm. Consequently, the best way to visualize the flow of gaseous CO_2 desorbing from champagne is to fit the IR video camera with a band-pass filter (centered on the CO_2 emission peak). The experimental device consists of a CEDIP middle waves Titanium HD560M IR video camera, coupled with a CO_2 filter (Ø 50.8 mm X 1 mm thick– Laser Components SAS). In comple-

http://dx.doi.org/10.5772/51956

ment, the technique involves an extended high-emissivity (0.97) blackbody (CI systems provided by POLYTEC PI), used at a controlled uniform temperature of 80°C, and placed approximately 30 cm behind the glass. The IR video camera was used at a 10 frames per second (fps) filming rate.

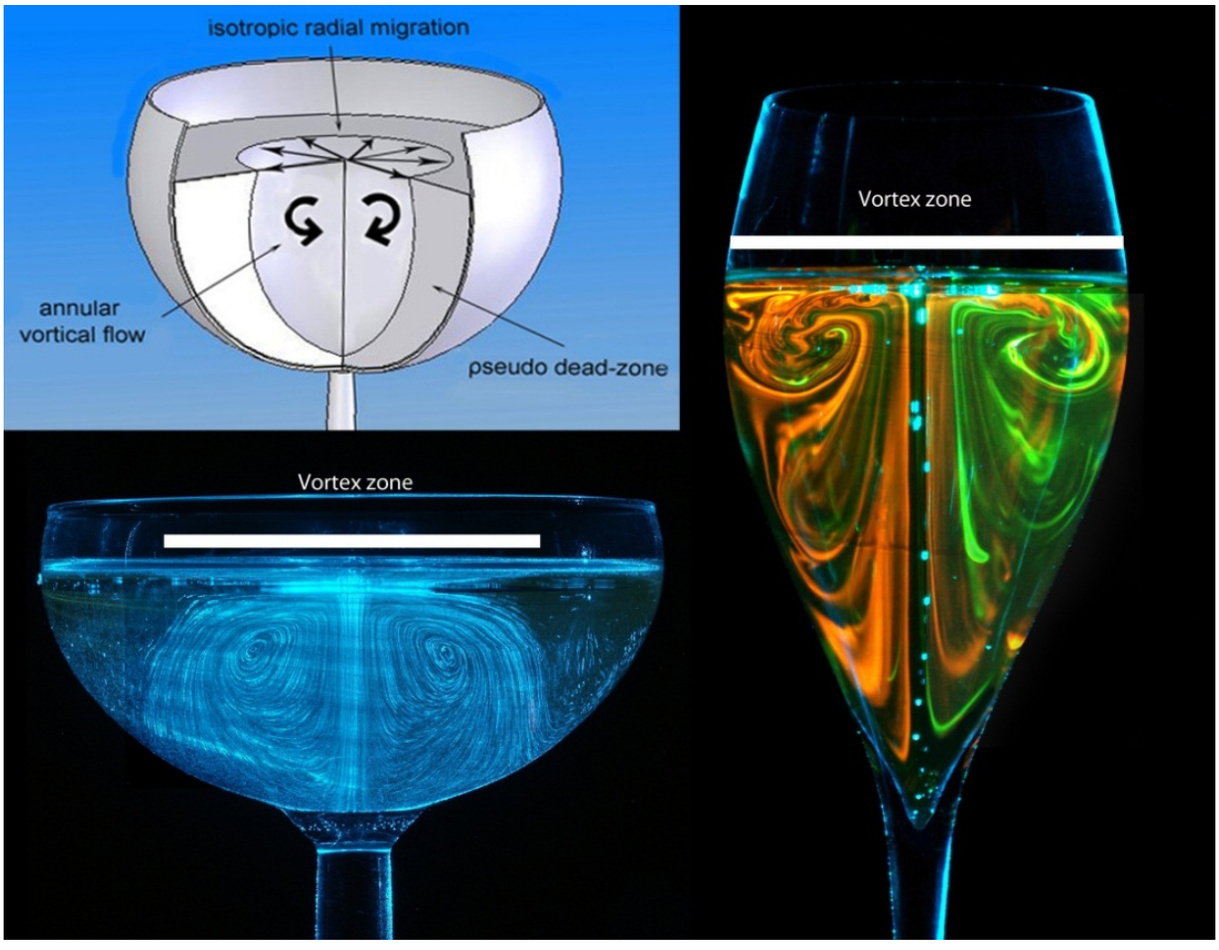

Figure 7. Glass shape and size have great influence on fluid flow and mixing in Champagne and sparkling wines. A flute imaged with fluorescent dye *(right)* shows that the resulting fluid vortex spans the entire width of the glass. A coupe glass, much shorter and wider, imaged with a laser and polymer particles, produces a similar vortex, but the vortex zone only extends across about half of the liquid *(bottom left).* A dead zone of no motion arises in the outer perimeter of the glass, and bubbles do not reach this area before bursting. A pseudo–dead zone beneath the liquid surface experiences only minimal movement and mixing *(top left).*

7. Results and discussion

7.1. Losses of dissolved CO2 during the service of champagne in each type of drinking vessel

As recently shown in a previous article, the pouring process is far from being inconsequential with regard to the concentration of CO_2 dissolved into the wine [11]. During the several

seconds of the pouring process, champagne undergoes highly turbulent and swirling flows. During this phase, champagne loses a very significant part of its initial content in dissolved CO_2. Gray scale infrared thermography time-sequences displayed in Figure 9 illustrate the progressive losses of dissolved CO_2 desorbing from the liquid phase into the form of a cloud of gaseous CO_2, whether champagne is poured in a flute or in a coupe. Clouds of gaseous CO_2 escaping from the liquid phase clearly appear. Consequently, at the beginning of the time series (i.e., at t=0, after the glass was poured with champagne and manually placed below the sampling valve of the chromatograph), champagne holds a level of dissolved CO_2 well below 11.6± 0.3 g L^{-1} (as chemically measured inside a bottle, after uncorking, but before pouring). In the present work, the initial bulk concentration of dissolved CO_2 after pouring, denoted c_i, was also chemically accessed by using carbonic anhydrase. To enable a statistical treatment, six successive CO_2 dissolved measurements were systematically done for each type of drinking vessel, after six successive pouring (from six distinct bottles). When served at 20°C,champagne was found to initially hold (at t=0, after pouring) a concentration of CO_2 dissolved molecules of $c_i^{flute} = 7.4\pm 0.4$ g L^{-1} in the flute, and $c_i^{coupe} = 7.4\pm 0.5$ g L^{-1} in the coupe (i.e., approximately 4 g L^{-1} less in both types of drinking vessel after pouring than inside the bottle, before pouring).

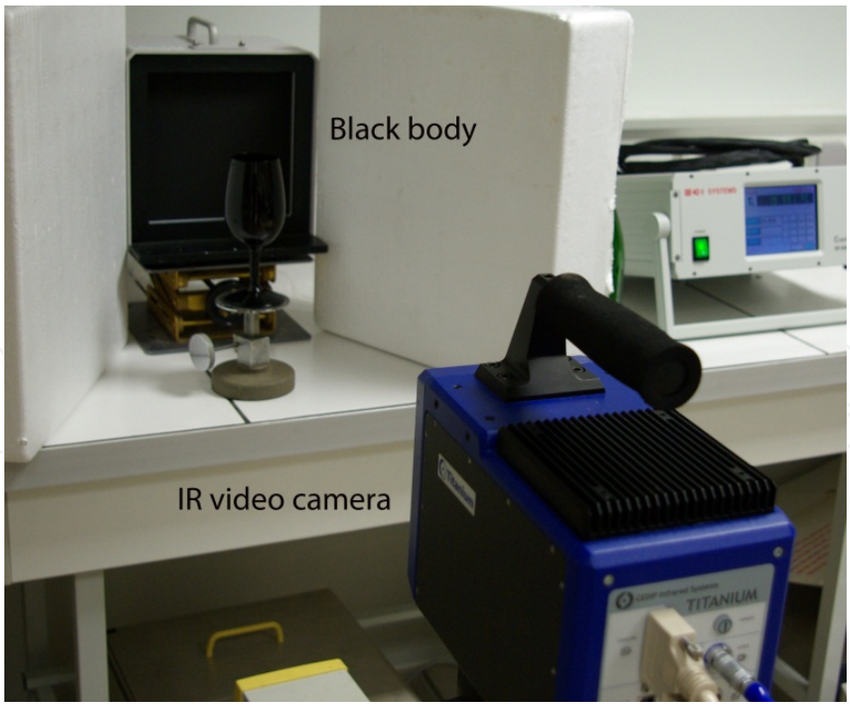

Figure 8. Experimental device

http://dx.doi.org/10.5772/51956

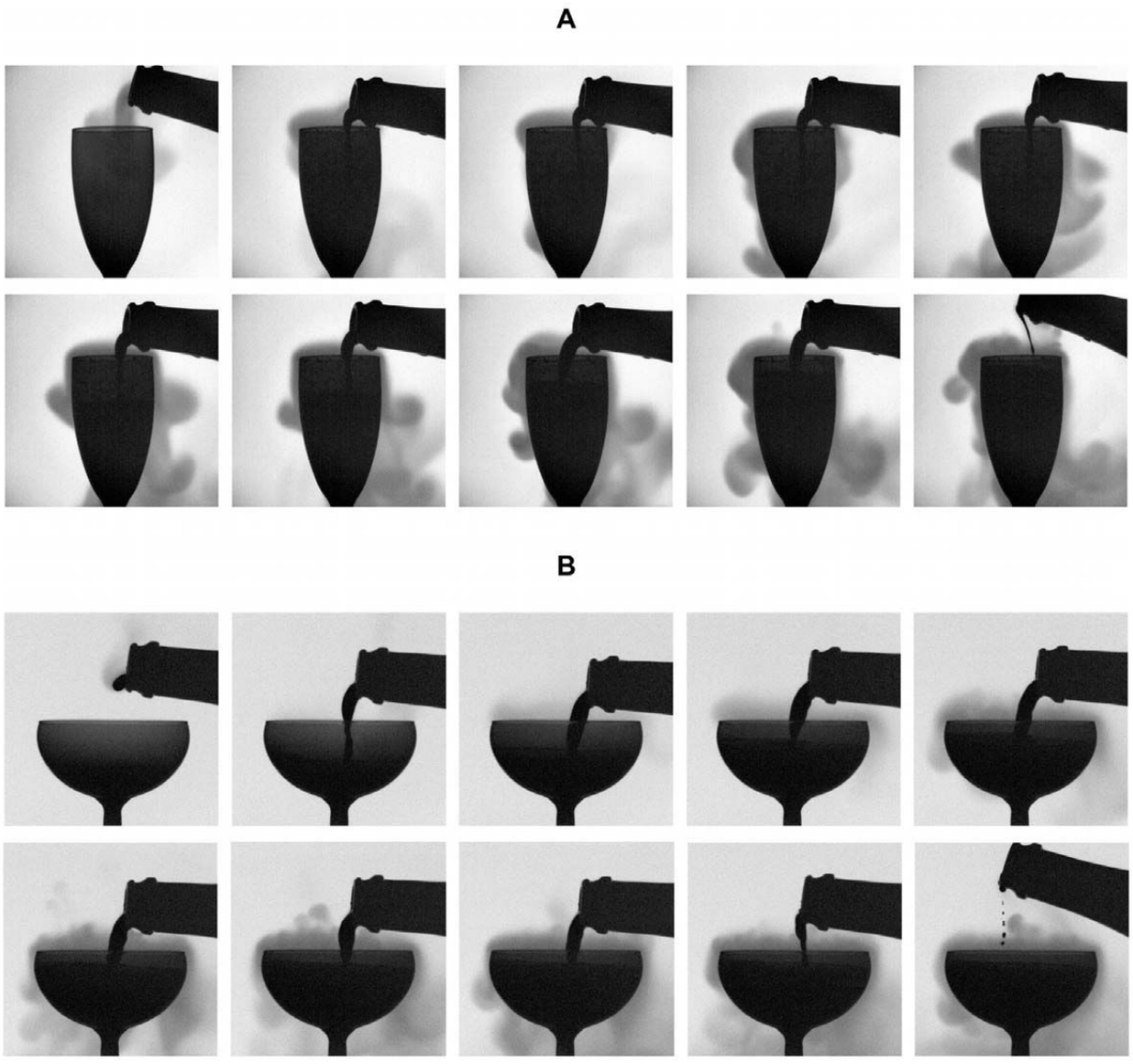

Figure 9. Infrared imaging of gaseous CO_2 desorbing when pouring champagne into both glass types. Gray scale time-sequences illustrating the pouring step as seen through the objective of the IR video camera – for a bottle stored at 20°C – whether champagne is served into the flute (a) or into the coupe (b).

7.2. Gaseous CO_2 and ethanol content found in the headspace above each type of drinking vessel

All along the first 15 minutes following pouring, concentrations of gaseous CO_2 found close to the edge of the flute are approximately between two and three times higher than those reached above the coupe. This observation is self-consistent with some recent data about volume fluxes of gaseous CO_2 measurements above glasses poured with champagne, including a flute and a coupe [11]. Fluxes of gaseous CO_2 per unit surface area offered to gas discharging are indeed significantly higher above the surface of the flute than above the surface of the coupe because the same total amount of dissolved CO_2 (<0.7 gram

for both glass types after pouring) has to be released by bubbles from a narrower surface, thus concentrating in turn more gaseous CO_2 in the headspace above the flute. Actually, due to higher concentrations of gaseous CO_2 above the flute than above the coupe, the smell of champagne, and especially its first nose, is always more irritating when champagne is served into a flute. It is indeed well-known that a sudden and abundant quantity of CO_2 (a strong trigeminal stimulus) may irritate the nose during the evaluation of aromas [12]. By using time-sequences provided through infrared imaging, the gaseous CO_2 desorbing from champagne and progressively invading the headspace above glasses was made visible in a false color scale (see Figure 10). Such an image processing analysis provides a better visualization of the relative differences in the CO_2 concentration field between both glass types, as shown in the thermography images displayed in Figure 11. Zones highly concentrated in gaseous CO_2 appear in black and dark blue, whereas zones slightly concentrated in gaseous CO_2 appear in red. The concentration of CO_2 found above the flute (close to the edge) is indeed always significantly higher than that found above the coupe. It can be noted for example, through infrared imaging, that the headspace (above the champagne surface, but below the glass edge) remains black during the first 3 min following pouring in case of the flute, whereas it progressively turns blue in case of the coupe.

Moreover, it is also worth noting from infrared imaging time-sequences that the cloud of gaseous CO_2 escaping from champagne tends to stagnate above the glass, or even tends to flow down from the edge of glasses by ''licking'' the glass walls (rather than diffuse isotropically around them). These observations conducted through infrared imaging betray the fact that gaseous CO_2 is approximately 1.5 times denser (ρ CO2$\approx$1.8 g L^{-1} *at* 20°*C*) than dry air is (ρ air$\approx$1.2 g L^{-1} *at* 20°*C*), and therefore tends to naturally flow down.

7.3. Numerical modeling of bubble induced flow patterns in champagne glasses

A numerical modeling of flow dynamics induced by the effervescence in a glass of champagne has been carried out for the first time using the finite volume method by CFD (Computational Fluid Dynamics). In order to define source terms for flow regime and to reproduce accurately the nucleation process at the origin of effervescence, specific subroutines for the gaseous phase have been added to the main numerical model. These subroutines allow the modeling of bubbles behavior based on semi-empirical formulas relating to bubble diameter and velocity or mass transfer evolutions. So, the idea of this study is to develop a "universal" numerical modeling allowing the study of bubble-induced flow patterns due to effervescence, whatever the shape of the glass in order to quantify the role of the glass geometry on the mixing flow phenomena and induced aromas exhalation process. Details and development of the steps of modeling are presented in this paper, showing a good agreement between the results obtained by CFD simulations in a reference case of those from laser tomography and Particle Image Velocimetry experiments, validating the present model.

http://dx.doi.org/10.5772/51956

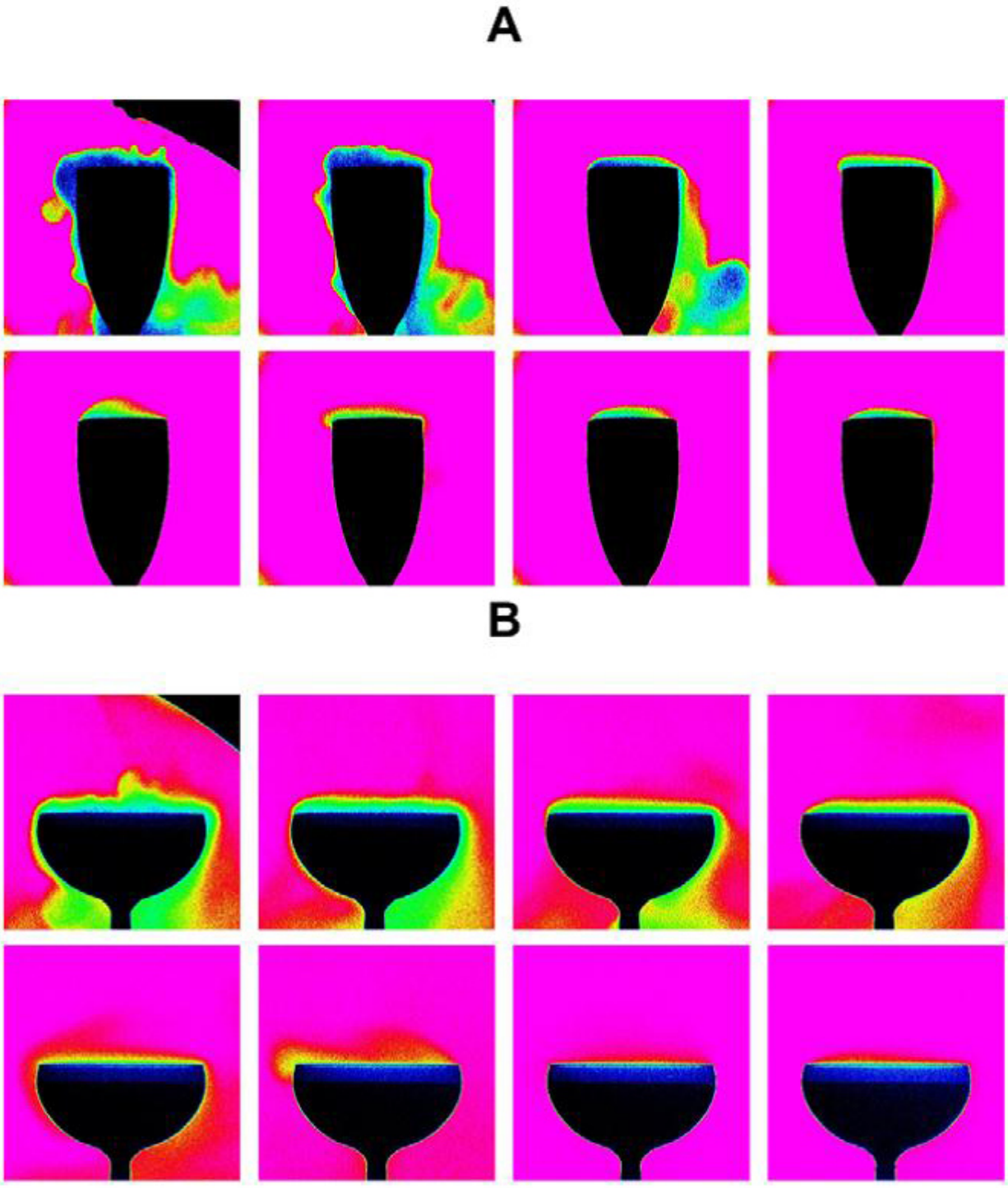

Figure 10. Infrared imaging of gaseous CO_2 desorbing from glasses filled with champagne. False color time-sequences illustrating champagne glasses as seen through the objective of the IR video camera, after the pouring step – for a bottle stored at 20°C –whether champagne is served into the flute (a) or into the coupe (b).Zones highly concentrated in gaseous CO_2 appear in black and dark blue, whereas zones slowly concentrated in gaseous CO_2 appear in red.

8. Geometry, equations and boundary conditions

8.1. Geometry and mesh generation

A traditional flute has been considered as a reference glass case. The glass geometry used in this study has been created from the real dimensions measured of the glass used for the experiments.

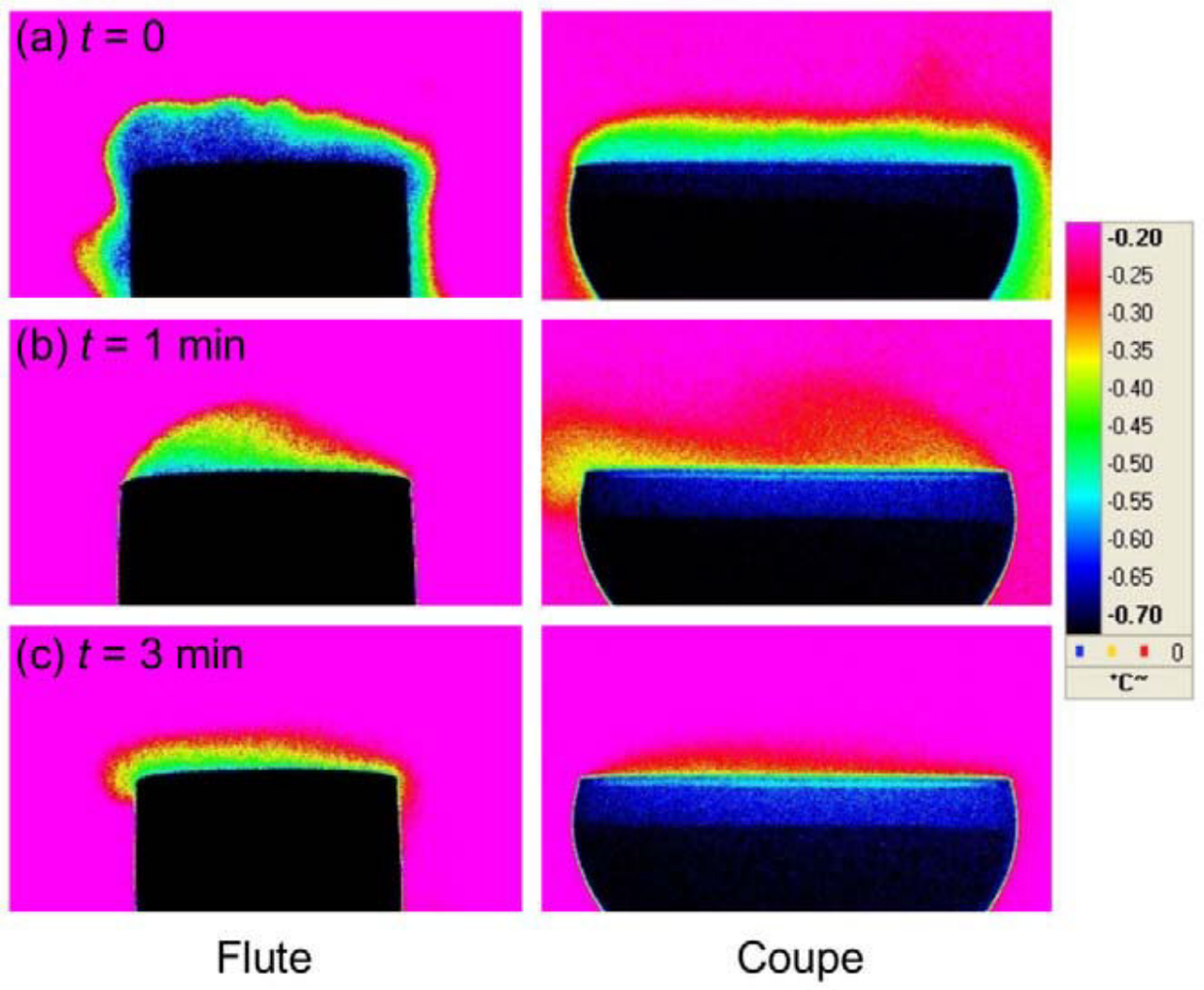

Figure 11. Close-up on gaseous CO_2 desorbing above both glass types. False color IR time-sequences showing close-up snapshots of CO_2 clouds desorbing above the flute and the coupe, respectively, immediately after pouring (a), 1 min after pouring (b), and 3 minutes after pouring (c); By using the color scale which provides a correspondence between the relative abundance of gaseous CO_2 and the temperature detected by the IR sensor of the camera after absorption by the gaseous headspace above glasses, it clearly appears that gaseous CO_2 is always more concentrated above the flute than above the coupe.

To ensure a continuous and perfectly controled process of effervescence, glassmakers usually consider circulary engraved glasses (figure 3). In such a way, as previously mentionned, the flow structure exhibits a quasi steady two dimensional behavior [2] (figures 6-7).

http://dx.doi.org/10.5772/51956

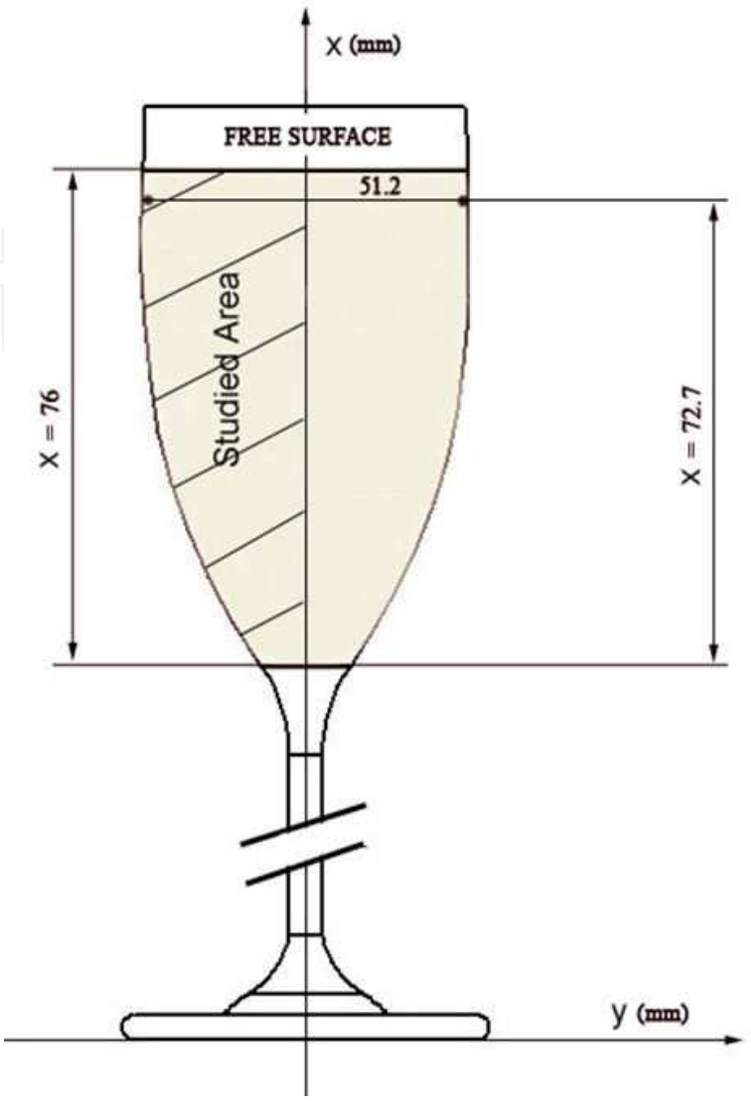

Figure 12. Champagne flute model.

In this situation, a 2D examination in the axis-symmetry plane can be considered as sufficient. For this purpose, only half of the studied area was drawn. The study area has a total height of 76 mm which corresponds to the fill level and its diameter is 51.2 mm at the liquid surface level (figure 12).

The ANSYS® Workbench Design Modeler software has been used to draw the geometry from the real size (scale 1:1) of the numerical study glass used as reference.

The mesh of the domain has been carried out using the ANSYS® Workbench meshing software. It consists in a two-dimensional mesh efficient in the case of simulations of axisymmetrical flow features. The body has been meshed with quadrilateral elements along the central part of the flow curvature, he is structured composed by square elements (L X L) but to follow the wall, the mesh is unstructured (figure 4).

8.2. Equations and numerical scheme

Because champagne is a wine in which as well gaseous as liquid phase are simultaneous present, the flows in a glass of champagne have been simulated numerically with a multiphase model. The flow is supposed laminar [6,14] and governed by the volume finite equations. The liquid phase hydrodynamics are described with the continuity and momentum conservation equations for laminar flows:

Continuity equation:

The general form of the continuity equation can be written as:

$$\frac{\partial \rho}{\partial t} + \nabla \bullet (\varrho \vec{v}) = S_m \tag{1}$$

The source S_m is the mass added to the continuous phase from the dispersed second phase.

For 2D axisymmetric geometries, the continuity equation is given by:

$$\frac{\partial \rho}{\partial t} + \frac{\partial}{\partial x}(\rho v_x) + \frac{\partial}{\partial r}(\rho v_r) + \frac{\rho v_r}{r} = S_m \tag{2}$$

where x is the axial coordinate, r is the radial coordinate, v_x is the axial velocity and v_r is the radial velocity.

Conservation of momentum is described by:

$$\frac{\partial}{\partial t}(\varrho \vec{v}) + \nabla \bullet (\varrho \vec{v} \vec{v}) = - \nabla p + \rho \vec{g} + \vec{F} \tag{3}$$

where ϱ is the static pressure and $\rho \vec{g}$ and $\vec{F}$ are the gravitational body force and external body forces (forces that arise from interaction between the liquid phase and the dispersed one).

For 2D axisymmetric geometries, the axial and radial momentum conservation equations are given by:

$$\frac{\partial}{\partial t}(\rho v_x) + \frac{1}{r}\frac{\partial}{\partial x}(r \rho v_x v_x) + \frac{1}{r}\frac{\partial}{\partial r}(r \rho v_r v_x) = - \frac{\partial \rho}{\partial x} + F_x \tag{4}$$

and

$$\frac{\partial}{\partial t}(\rho v_r) + \frac{1}{r}\frac{\partial}{\partial x}(r \rho v_x v_r) + \frac{1}{r}\frac{\partial}{\partial r}(r \rho v_r v_r) = - \frac{\partial \rho}{\partial r} + F_r \tag{5}$$

where

http://dx.doi.org/10.5772/51956

$$\nabla \bullet \vec{v} = \frac{\partial v_x}{\partial x} + \frac{\partial v_r}{\partial r} + \frac{v_r}{r} \tag{6}$$

In this work, we hve used the Lagrangian-Eulerian approach which analyzes the liquid phase (primary phase) by the Eulerian method and the bubble phase (secondary phase) by Lagrangian assumption allowing the monitoring of bubbles life cycle.

The Euler-Lagrange approach is the basis of the lagrangian discrete phase model. The dispersed phase is solved by tracking the bubbles through the calculated flow domain while the fluid phase is treated continuously by solving the Navier-Stockes equations. Exchanges of momentum and mass are realized between the dispersed phase and the fluid one.

According to the lagrangian multiphase model, the volume fraction of the discrete phase (secondary phase) is quite small.

The bubbles trajectories are computed individually at each time step during the fluid phase calculation. This model is perfectly adapted for modeling the flows in a glass of champagne. In order to reproduce as closely as possible the principle of nucleation, subroutines have been used for the gaseous phase. These subroutines have been written based on physical laws that are taken from experimental results [5, 6].

The trajectory of a bubble is predicted by integrating the force balance in a Lagrangian reference frame.

During its rise in the liquid, a bubble is subjected to the action of several forces [14]:

The buoyancy:

$$F_B = \frac{4}{3}\pi R^3 \rho g \tag{7}$$

The drag force F_D which is related to the fluid flow around the bubble, when the bubble begins to move the fluid that is around it. The movement of the surrounding fluid leads to an additional force F_{MA} called "added mass" related to the variation in the amount of movement of liquid displaced:

$$F_{MA} = \frac{\rho d}{dt}(Vu) \tag{8}$$

The volume V of liquid entrained in the wake of the bubble is roughly equal to the half of the volume of the bubble. Thus:

$$F_{MA} = \frac{2}{3}\rho\pi\frac{d}{dt}(R^3 u) \tag{9}$$

The equation of motion can be written:

$$\frac{2}{3}\rho\pi R^3\left(\frac{dU}{dt}+\frac{3U}{R}\frac{dR}{dt}\right)=\frac{4}{3}\pi R^3\rho g-\frac{1}{2}C_D\rho U^2\pi R^2 \tag{10}$$

The force of added mass has been compared to the buoyancy along the path of the bubble to the surface. The force of added mass does not exceed 2-3% of the buoyancy, so it can be neglected in the remainder of the study. The equation of motion is finally reduced to a simple equality between the drag force and buoyancy.

In this case, the drag force F_D is defined as

$$F_D=\frac{1}{2}C_D\rho u^2\pi R^2 \tag{11}$$

where C_D is the drag coefficient. During ascent, surface active materials progressively accumulate at the rear part of the rising bubble, thus increasing the immobile area of the bubble surface.

Arising bubble rigidified by surfactants runs into more resistance than a bubble presenting a more flexible interface free from surface-active materials. The champagne bubbles showed therefore a behavior intermediate between that of a rigid and that a fluid sphere. To take into account the surfactants accumulation, the two following experimental drag coefficients laws, available in the range of intermediate Reynolds numbers (10^{-1} *to* 10^2) covered by champagne bubbles, have been used.

Magnaudet et al [14] have proposed a semi empirical relationship between the drag coefficient and the Reynolds number:

$$C_D=\frac{16}{Re}\left(1+0.15\sqrt{Re}\right)\qquad(Re<50) \tag{12}$$

This experimental determination of the drag coefficient for fluid spheres is available for Reynolds number less than 50.

Since the Reynolds number exceeds the limit of 50 for sufficiently long path, another empirical law has been used available for $Re>50$, determined by *Maxworthy et al* [14]

$$C_D=11.1Re^{-0.74}\qquad(1<Re<800) \tag{13}$$

Because bubbles do not exceed a critical diameter of 2 mm, they are spherical during their ascent. Moreover, the assumption that the bubbles do not coalesce or breakup has been considered.

The Reynolds number is defined by:

$$R_e=\frac{2\rho Ru}{\eta} \tag{14}$$

http://dx.doi.org/10.5772/51956

The density and the viscosity of the champagne wine for the liquid phase and the density and the viscosity of the carbon dioxide for the gaseous phase have been stored in the materials database (table 1).

The numerical simulations have been carried out with the ANSYS FLUENT® software using volume finite approach. The convergence criteria were based on the residuals resulting from the integration of the conservation equations over finite control-volumes. During the iterative calculation process, these residuals were constantly monitored and carefully scrutinized. For all simulations performed in this study, converged solutions were usually achieved with residuals as low as 10^{-5} (or less) for all the governing equations. To carry out numerical simulations on the dynamics of the fluid, a structured mesh, whose dimensions are 0.2 x 0.2 mm², has been chosen in the main central part of the domain where bubbles are present.

9. Boundary conditions

Models based on classical nucleation theory do not give a satisfactory approach of nucleation in the effervescent wines [13]. The idea has been to create routines to simulate the principle of nucleation and then compare the results with those obtained with experimental data [5, 6]. In order to simulate the bubbles growth, the bubbles velocity, the mass transfer between bubbles, the mass flow rate and the drag law, we have written User Defined Functions (UDF) in C language which defines source terms for the flow regime. The variation of bubbling frequency, which is a function of the CO_2 dissolved concentration, is made possible by changing the time step during the calculation.

The radius R(m) of champagne bubbles increase in time at a constant growth rate $k = \frac{dR}{dt}$, as bubbles rise toward the liquid surface. Thus, $R(t) = R_0 + kt$ where R_0 is the bubble radius as it detaches from the nucleation site.

The semi-empirical growth rate (k, μm/s) of bubbles rising in champagne was linked with some physicochemical properties of liquids as follows [5, 6]:

$$k = \frac{dR}{dt} \approx 0.63 \frac{R_\theta}{P_0} D_0^{\frac{2}{3}} (2\alpha\rho g / 9\eta)^{1/3} (C_L - k_H P_0) \quad (15)$$

The bubbles diameter depends on both the distance to the surface H (m) and the growth rate k (μm/s) which decreases over time. The law governing the change in radius R(m) of a bubble is [5, 6]:

$$R \approx 3\left(\frac{\eta}{2\alpha\rho g} kH\right)^{1/3} \quad (16)$$

Where α is a numerical coefficient that depends on the fluid in question, estimated to be 0.7 in the case of sparkling wines [5, 6].

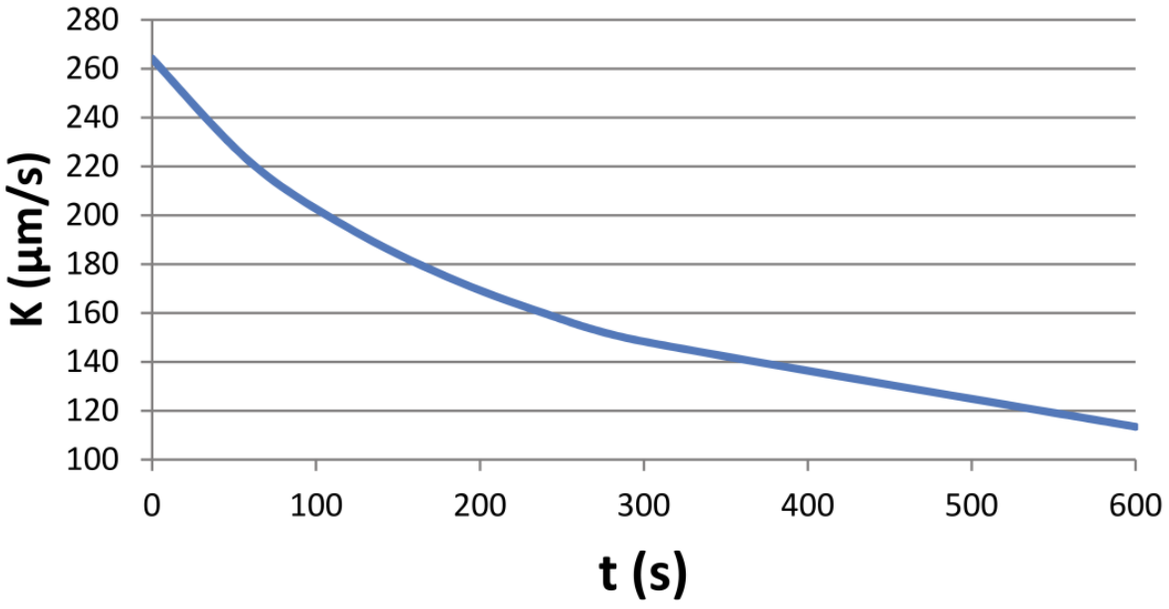

Figure 13. Evolution of the bubble growth rate according to time after pouring.

The bubbles velocity u(m/s) varies according to the following expression [6, 14]:

$$u \approx \frac{2\alpha\rho g}{9\eta} R^2 \tag{17}$$

This factor accounts the rigidity of the bubble and thus the braking effect due to the presence of surfactant molecules on the surface of bubbles. It will be smaller if the bubble is made rigid by a thick shield of surfactant molecules.

The mass flow rate Q_m (kg/s) is defined by:

$$Q_m = \frac{N}{t} \times \rho_p \times V_b \tag{18}$$

The CO_2 dissolved concentration C_L decreases continuously over time once the wine is poured into the glass. This parameter also varies with the temperature. In this study, we have used the champagne physicochemical parameters at 20° C corresponding to our reference temperature for the experiments (**Table 1**).

	Champagne (20°C)	Carbon dioxide (20°C)
Density (kg/m^3)	998	1.7878
viscosity (kg/m/s)	0.00166	$1.37 \cdot 10^{-5}$
Surface tension (N/m)	0.0468	0

Table 1. Physicochemical parameters of Champagne and Carbon dioxide (from [14]).

10. Numerical results

The results obtained by numerical simulation have been compared with those from experiments using two flow visualization techniques to get both qualitative and quantitative viewpoints (figure 14) [2-5]. The laser tomography as a qualitative analysis method has been used to visualize the flow patterns and vertical structures induced by the continuous column of ascending bubbles in the reference flute poured with champagne. A comparison of the flow feature is presented in Figure 9. During the time-exposure of a camera, the liquid seeded with solid Rilsan particles [2-5, 7-8] and lighted by a planar laser sheet exhibits streamline patterns (figure 14b). Comparison between these experimental streamlines and the numerical ones (figure 14a) shows a good agreement, especially regarding to the location of the vortex cores in the investigated domain. The global flow features are satisfactory modeled with the CFD developed code.

To highlight a quantitative validation of the numerical modeling, velocity profiles as well velocity profiles as velocity iso-contour maps have been interested. The experimental data have been obtained by Particle Image Velocimetry measurements [15]. Figure 15 presents a comparison between the two experimental and CFD velocity profiles drawn for a 72.7mm X-location. The general trend is well reproduced as well for the X-velocity peak on the axis of symmetry as for the return flow characterized by negative velocity X-component values. Curve extrema are located at the same Y-location. Numerical results are in good accordance with those obtained by PIV measurement for the velocity profiles. Similar conclusions have been deduced for other X-locations (not presented here).

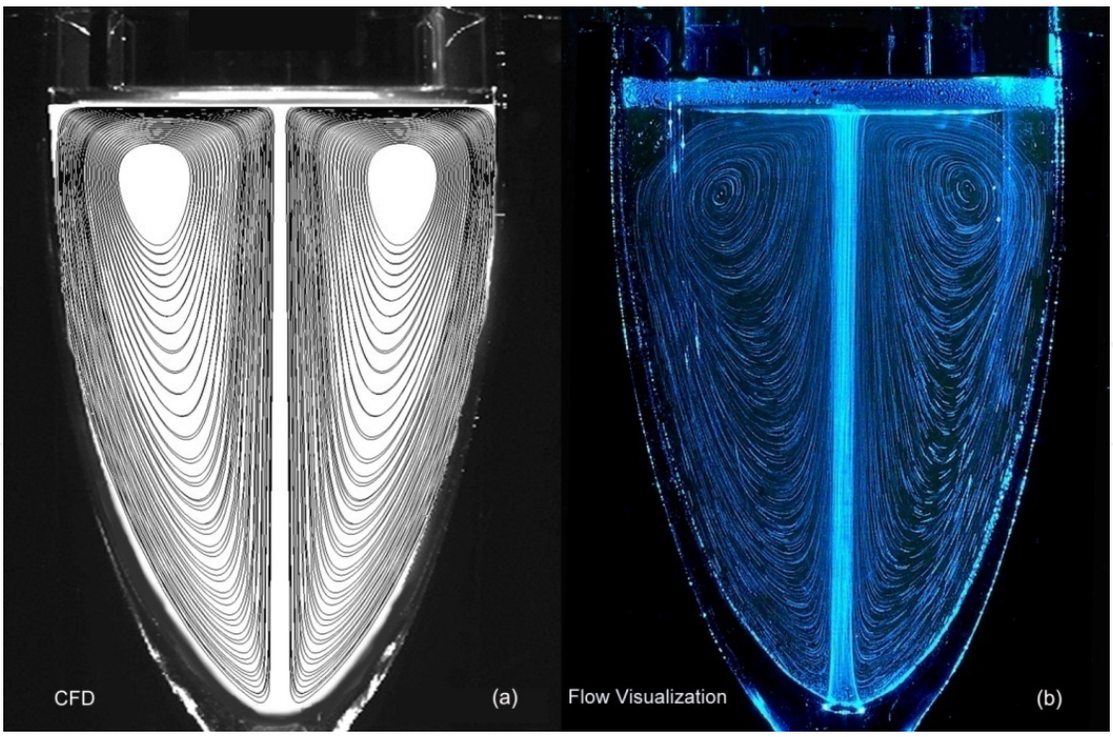

Figure 14. Streamlines obtained by CFD simulation (a) compared with classic flow visualization (b) at t = 5 minutes following the pouring process.

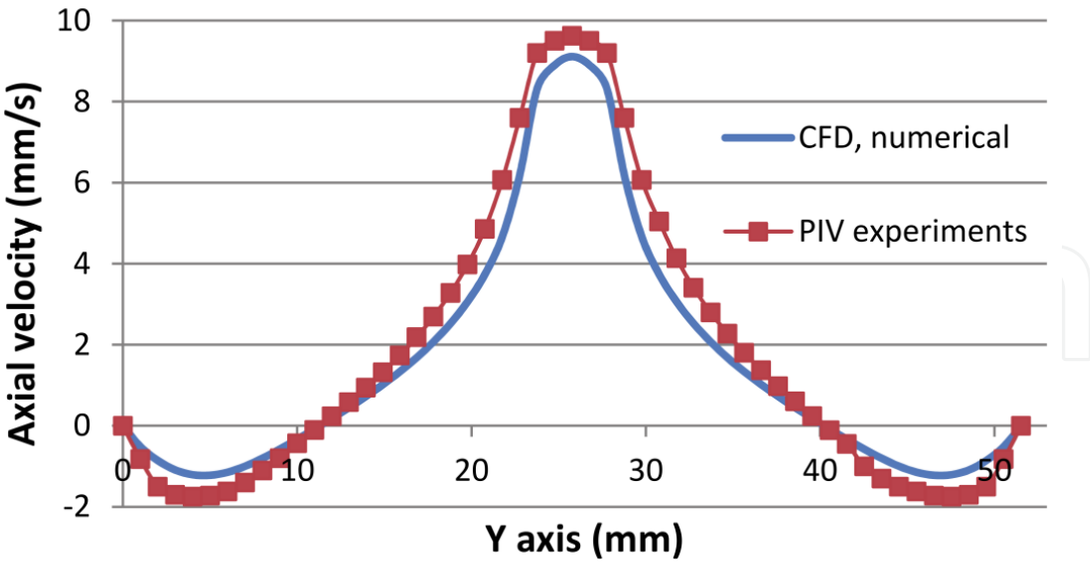

Figure 15. Axial velocity of liquid phase at t = 1 minute after pouring process and X = 72.7 mm, comparison between PIV measurement and CFD simulation.

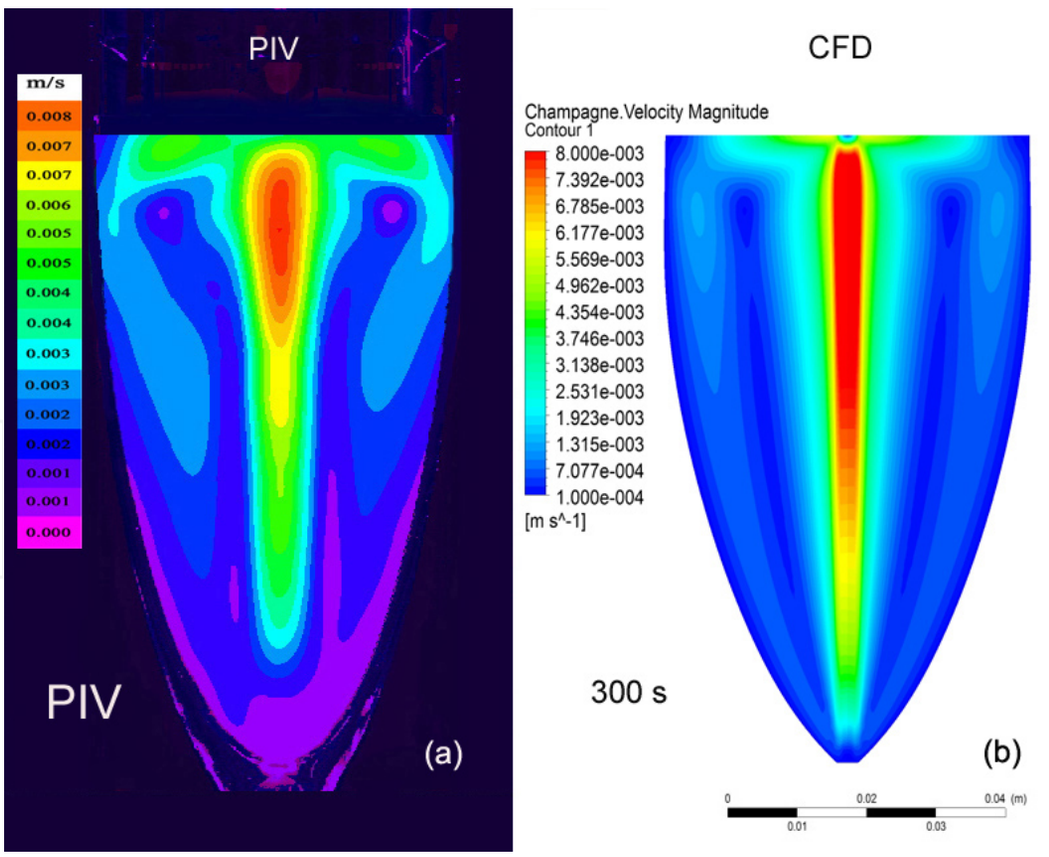

Figure 16. PIV measurements (a) compared with CFD simulation (b) at t = 5 minutes after pouring process, velocity magnitude of the liquid phase.

Velocity-magnitude maps are drawn in figure 16 for the two numerical and PIV-measurement approaches. A close agreement appears on the two maps. A same maximum velocity magnitude whose value is 8 mm/s is observed at the same location on the central part of the flow. Similar comments can be drawn concerning the vortex cores locations. Even if iso-contour curves differ a little bit, the trend is duplicated on these two maps and the estimated velocity is the same order of magnitude as those measured by experimental one.

Thus, one can conclude that the numerical simulation allows a satisfactory approach of the fluid dynamics.

11. Conclusion

A classical flow visualization technique was used in order to capture the fluid motion in traditional flutes and coupes poured with champagne. It was found that glasses engraved around their axis of symmetry produce a rising gas column along the vertical glass axis which induces, in turn, recirculating flow regions. In case of the classical engraved champagne flute, the whole domain of the liquid phase is homogeneously mixed, whereas in the case of the engraved champagne coupe, the recirculating flow region does not occupy the whole volume in the glass. In the engraved coupe, a "dead-zone" of no motion was identified which inhibits the formation of the collar at the glass edge. Because the kinetics of flavor and gas release also strongly depend on the velocity of the recirculating flows close to the interface, we therefore strongly believe that this paper brings objective elements and clues in order to better understand the role of glass shape and engravement conditions on the "olfactive" behavior of champagne and sparkling wines in a glass. To go further; a developed gaseous CO_2 visualization technique based on infrared imaging was performed. Those analytical results are self-consistent with sensory analysis of champagne and sparkling wines, since it is generally accepted that the smell of champagne, and especially its first nose, is always more irritating (because more concentrated in gaseous CO_2 which is a strong trigeminal stimulus) when champagne is served into a flute than when it is served into a coupe. In addition, a numerical modeling of flow dynamics induced by effervescence in a glass of champagne has been carried out for the first time in order to quantify the role of the glass geometry on the mixing flow phenomena and induced aromas exhalation process.

Appendix

C_D drag coefficient (dimensionless)

C_l lift coefficient (dimensionless)

C_L CO_2 dissolved concentration in the liquid (g/l)

D_0 diffusion coefficient of CO_2 molecules (m^2 / s)

F_D drag force

g acceleration due to gravity (m.s^{-2})

H liquid height (m)

k theoretical growth rate of bubbles (μm/s)

L characteristic dimension of a mesh element (mm)

N bubbling frequency (H_Z)

P_0 atmospheric pressure (atm)

Q_m mass flow rate (kg/s)

R bubble radius (m)

R_e Reynolds number (dimensionless)

u bubble velocity (m/s)

v liquid velocity (m/s)

V_b bubble volume (m^3)

R ideal gas constant (8.31 J/mol/K)

ρ liquid density (kg/m^3)

ρ_p density of CO2 (kg/m^3)

η dynamic viscosity (kg/m/s)

α numerical coefficient (dimensionless)

θ liquid temperature (°C)

λ molecular mean free path (m)

ϕ bubble diameter (m)

Author details

Fabien Beaumont[1], Gérard Liger-Belair[2] and Guillaume Polidori[1*]

1 GRESPI/Thermomécanique, Université de Reims, France

2 GSMA, UMR CNRS 7331, Université de Reims, France

References

[1] Liger Belair G., Cilindre C., Gougeon R.D., Lucio M., Gebefügi I., Jeandet P., Schmitt-Kopplin P., Unraveling different chemical fingerprints between a champagne wine and its aerosols, PNAS 2009, volume 106, n°39, 16545-16549.

[2] Polidori G., Jeandet P., Liger-Belair G., Bubbles and flow patterns in Champagne, American Scientist 2009, 97, 294.

[3] Liger Belair G., Religieux J.-B., Fohanno S., Vialatte M.-A., Jeandet P., Polidori G., Visualization of mixing phenomena in champagne glasses under various glass-shape and engravement conditions, J. Agric. Food Chem 2007, 55, 882.

[4] Polidori G., Beaumont F., Jeandet P., Liger Belair G., Artificial bubble nucleation in engraved champagne glasses, J. Visualization 2008, 11-4, 279.

[5] Liger Belair G., Polidori G., Jeandet P., Recent advances in the science of champagne bubbles, Chem. Soc. Rev. 2008, 37, 2490.

[6] Liger Belair G., Ann.Phys 2002. (Paris) 27, 1.

[7] Polidori G., Beaumont F., Jeandet P., Liger Belair G., Ring vortex scenario in engraved Champagne glasses, J. Visualization 2009, 12-3, 275.

[8] Polidori G., Beaumont F., Jeandet P., Liger Belair G., Visualization of swirling flows in champagne glasses, J. Visualization 2008, 11-3, 184.

[9] Liger Belair G., Beaumont F., Jeandet P.and Polidori G., Flow patterns of bubble nucleation sites (called fliers) freely floating in champagne glasses, Langmuir 2007, 23, 10976.

[10] Liger-Belair G, Bourget M, Villaume S, Jeandet P, Pron H, et al., On the losses of dissolved CO2 during champagne serving, J Agric Food Chem 2010, 58: 8768–8775.

[11] Liger-Belair, G., Villaume, S., Cilindre, C., Jeandet, P., CO2 volume fluxes outgassing from champagne glasses: The impact of champagne ageing, Analytica Chimica Acta 2010, 660, 29–34.

[12] Duteurtre B, Le Champagne: de la tradition à la science 2010. Paris: Lavoisier. 384 p.

[13] Herrmann E., Lihavainen H., Hyvärinen A.P., Riipinen I., Wilk M., Stratmann F., Kulmala M., Nucleation Simulations using the fluid dynamics software FLUENT using the Fine Particle Model FPM, The Journal of physical chemistry 2006, A 2006, 110, 12448-12455.

[14] Liger Belair G., Marchal R., Robillard B., Dambrouck T., Maujean A., Vignes-Adler M., Jeandet P., On the Velocity of Expanding Spherical Gas Bubbles Rising in Line in Supersaturated Hydroalcoholic Solutions: Application to Bubble Trains in Carbonated Beverages, Langmuir 2000, 16, 1889-1895.

[15] Liu Z., Zheng Y., Jia L., Zhang Q., Study of bubble induced flow structure using PIV , Chemical Engineering Science 2005, 60, 3537-3552.

IntechOpen